RSC Advances

PAPER

View Article Online
View Journal | View Issue

Cite this: *RSC Adv.*, 2021, **11**, 9775

Hybrid structure of MWCNT/ferrite and GO incorporated composites for microwave shielding properties and their practical applications†

Sumit Kumar,[ab] Rajan Walia,[c] Ashwani Kumar[d] and Vivek Verma *[b]

To eliminate the increasing adverse effects of electromagnetic pollution in everyday life, the shielding abilities of ferrite nanoparticles, multiwalled carbon nanotubes, and graphene oxide based hybrid composites have been investigated. The conceivable applications of the best investigated shielding composite samples on wearable and construction materials were investigated. Zinc substituted nickel and cobalt ferrite nanoparticles were synthesized using a sol–gel method with average crystallite size of 15–20 nm and incorporated with MWCNT and MWCNT–GO in a 1 : 1 weight ratio. Detailed investigations have been done on the prepared nano-composites by using X-ray diffraction, scanning and transmission electron microscopy, Fourier-transform infrared spectroscopy (FTIR), thermogravimetric analysis, magnetic hysteresis loops, and vector network analysis. The microwave shielding capacity of the multiwalled carbon nanotube-zinc doped cobalt ferrite–graphene oxide hybrid composite was significantly enhanced up to 81.6 dB for the thickness of 2.4 mm in the X-band frequency region. Such a high SE indicates attenuation of the entire incoming EM radiation, which corroborates the potential of these materials in terms of high efficiency, tuneable, stable, and lightweight shielding applications. The synthesized MWCNT–CZFO–GO nanocomposite was used as an absorbent and was incorporated with cotton fabric, camouflage fabric, cement, and gypsum for high-efficiency daily life radiation shielding applications. These incorporated shielding samples (52.3 dB for cement, 31.4 dB for gypsum, 40.8 dB for camouflage fabric, and 28.6 dB for cotton fabric) showed a high attenuation capacity with more than 99.999% attenuation of the incident EM radiation establishing a promising behaviour to neutralize the harmful effects of radiation in day-to-day life.

Received 10th February 2021
Accepted 1st March 2021

DOI: 10.1039/d1ra01129d

rsc.li/rsc-advances

1. Introduction

We are currently living in an environment which is completely based on the large scale use of much developed and advanced communication technology, various kinds of electronic gadgets or instruments to make our life very convenient and easy. But this advancement of technologies has teamed up with a new kind of pollution called Electromagnetic Interference due to the excessive presence of undesired electromagnetic radiation in the environment which not only degrades and adversely affects the performance and accuracy of electronic devices but also has hazardous effects on both living and non-living species.[1] Image wavering or sound alterations in television, radios and computer screens, the interconnection of signal lines in mobile communications, and disfunctioning of wireless devices by interruption of various electrical, radio, or satellite signals are some examples of EMI in our day-to-day life.[2,3] Hence over the past years, EMI shielding materials possessing properties like low density, lightweight, less thickness, strong absorption capacity and large bandwidth, which convert the unwanted EM energy into thermal or other forms of energy have gained high significance by either reflection or absorption of incident radiations.[4,5] Metals, even though the most traditional EM shielding materials, possess many disadvantages such as high density, poor corrosion resistance, and complex processing. The electromagnetic interference shielding behaviour of various materials such as polymer composites, carbon materials, ferrites, ceramics and 2D materials have also been studied in order to achieve high shielding effectiveness (SE). As a prerequisite to process materials with high shielding effectiveness, it is essential to explore carbon-based materials which when mixed with different absorbers, can be used to fabricate lightweight and highly efficient shielding materials. The shielding effectiveness (SE) of these conducting carbon materials mainly originates from the reflection phenomena of incident EM

[a]*Department of Physics and Astrophysics, University of Delhi, Delhi, India*
[b]*Department of Physics, Hindu College, University of Delhi, Delhi, India. E-mail: vermavivek.neel@gmail.com; vivekverma@hinducollege.ac.in*
[c]*Department of Physics, Deen Dayal Upadhyaya University, Gorakhpur, Uttar Pradesh, India*
[d]*Nanoscience Laboratory Institute Instrumentation Centre, IIT Roorkee, India*

† Electronic supplementary information (ESI) available. See DOI: 10.1039/d1ra01129d

radiations on the surface of materials.[6] Carbon nanotubes (CNTs) and graphene-based fillers are predominantly considered as potential candidates for designing microwave shielding due to their conductivity, high aspect ratios and skin effects, leading to a high-frequency bandwidth.[7–9] Multiwall carbon nanotubes have unique structural arrangements possessing small diameter, high aspect ratio, high electrical conductivity and good tensile strength, which makes them promising candidates in designing for high shielding capacity applications.[10,11] Graphene oxide (GO) due to its superior mechanical, thermal, electrical, chemical and optical properties with the presence of defect sites and attached functional groups, can serve as low density, high mechanical strength and efficient shielding material.[12] The C–C interfacial layers in the MWCNT or GO based composite materials create uneven electronic structures, which attenuate the transmission of EMWs in the materials. EM wave absorbing materials which can be used as fillers to the carbon materials, shield the devices more efficiently by converting the incident EM wave energy into thermal energy with the help of electric and/or magnetic losses and dissipating it through the surface.[13,14] Shielding strength of any material is determined by the term called shielding effectiveness (SE) which depends on the dielectric strength of the material, the magnetic permeability of the material, thickness of shield and frequency of incident radiations. Since, both CNT and GO possess low magnetic response or nonmagnetic nature due to which the presence of magnetic losses which are responsible for absorption of incident EM radiations are very less. Therefore, to enhance the absorption of the incident EM radiations, ferrite nanoparticles can be embedded to host carbon materials-based matrices which leads to the formation of composites having both electric and magnetic losses.[15,16] In a common process, the carbon-based materials possess high electric loss capacity to the incident electromagnetic wave while the electromagnetic losses in ferrites are generally because of their high magnetic absorption.[17–19] In our earlier works, we also have studied the effect of different ferrite nanomaterials (cobalt, nickel, zinc and zinc doped ferrites) along with conducting polyaniline and we have found that saturation magnetization of ferrite nanoparticles, their dispersibility and thickness of materials play a major role in achieving the high shielding effectiveness.[20] In the current study, we dealt simultaneously with both electrical losses and magnetic losses by incorporating ferrite nanoparticles into multiwalled carbon nanotubes and a hybrid phase of both with graphene oxide to propose lightweight hybrid composite materials with highly efficient EMI shielding. So, to achieve the high shielding absorption response, we have taken the modified composition of cobalt ferrite and nickel ferrite. Zn doped nickel and cobalt ferrite nanopowders ($Ni_{0.7}Zn_{0.3}Fe_2O_4$ and $Co_{0.7}Zn_{0.3}Fe_2O_4$) exhibits the optimum magnetic properties.[20–22] High shielding effectiveness of 81.6 dB at 10 GHz for a thickness of 2.4 mm was achieved for MWCNT–CZFO–GO composite sample. This composite material was further incorporated into cotton fabric, camouflage pattern fabric, cement and gypsum to explore the possible shielding applications in defence, daily life *etc.* As the increasing EMI pollution is imposing adverse effects on human health, so to secure the life sustainability we tried to gain high shielding through the basic wearable and construction materials which are of most common use and applicability. Cement and gypsum are elementary construction materials regularly used in daily life in every field of the community while the fabrics are also an essential entity for the human being used in various forms and various ways. Hence, the composite samples of MWCNT–ferrites–GO may be useful to reduce the electromagnetic interference effect and good candidate to suppress the radiation in environment.

2. Experimental methods

2.1 Materials

Ammonium hydroxide solution, nickel nitrate ($Ni(NO_3)_2 \cdot 6H_2O$), zinc nitrate ($Zn(NO_3)_2 \cdot 6H_2O$), ferric nitrate ($Fe(NO_3)_3 \cdot 9H_2O$), cobalt nitrate ($Co(NO_3)_2 \cdot 6H_2O$), citric acid and dimethylformamide (DMF) of analytical purity have been obtained from Fischer Scientific (India). Multiwalled carbon nanotubes (MWCNTs, $d = 9.5$ nm, $l = 1.5$ μm) and graphene oxide nanopowder were acquired from Ultra nanotech private limited (India). Cotton fabric, camouflage fabric, cement and gypsum were purchased from local sources.

2.2 Synthesis of ferrite nanoparticles

Nanoparticles of $Ni_{0.7}Zn_{0.3}Fe_2O_4$ (NZFO) and $Co_{0.7}Zn_{0.3}Fe_2O_4$ (CZFO) were synthesized by using the sol–gel method. Nitrate precursors were separately dissolved in de-ionized water in appropriate stoichiometric amounts for homogenous mixing of the precursors on the magnetic stirrer. Then, the citric acid was added to the solution as complexing agent with equal molar ratio to the total metal nitrate precursors under the constant stirring. The pH of the solution was adjusted to 7 using ammonia solution. The resulting solution was then evaporated at about 70 °C until the transparent sol obtained. Then the solution was further heated with the stirring till it became viscous and brown gel was formed. The brown gel then further attained dry state and very fragile foam was obtained with an exothermic reaction which was further grinded to obtain fine powder. The fine powders so obtained were finally calcined at 450 °C for 1 hour to conquer phase formation of ferrite nanoparticles in crystalline form.

2.3 Synthesis of composite materials

Composite samples were chemically synthesized by incorporating ferrite nanoparticles to host MWCNT matrix with 1 : 1 weight ratio for MWCNT–NZFO, MWCNT–CZFO samples and 0.5 : 1 : 0.5 for GO–NZFO–MWCNT and GO–CZFO–MWCNT which helps in achieving the impedance matching for both electric and magnetic losses and also enhance the interfacial phase interaction. Firstly, the MWCNTs and graphene oxide nanopowder were uniformly dispersed in the DMF solution through the ultrasonication method for 2–3 hours. Then, the ferrite nanoparticles were dissolved to the solution in appropriate weight ratio by magnetic stirring in the DMF mixture. The obtained solution was then centrifuged with deionized water

several times and then dried and grinded to synthesize the final phase composite materials. All the composite samples were synthesized in the same manner except that in the next two composites graphene oxide was also sonicated with the MWCNT solution in order to form a three phase composite material. GO–CZFO–MWCNT sample was further deposited on two different kind of fabrics by dipping in the solution the sample for about 24 hours. The fabric pieces were then brought out from the solution, washed with distilled water and further dried at room temperature for about 2–3 hours. In order to minimise the wide spreading EM pollution in daily life having adverse effects on human sustainability, we tried to develop EM shielding efficient constructions materials which can control the unwanted radiations present in environment. For this purpose, GO–CZFO–MWCNT nanocomposite sample was mechanically blended with the cement and gypsum in 1 : 1 weight ratio about 5–6 hours for each sample in order to obtain a homogenous composition.

3. Results and discussions

3.1 X-ray diffraction analysis

X-ray diffraction measurements were performed in order to examine the phase formation, crystalline nature and structural analysis of all the samples. Fig. 1(a) represents the XRD patterns of all pristine samples or the precursors which are required for synthesis of composites *i.e.* multiwalled carbon nanotubes, graphene oxide and ferrite nanoparticles. Fig. 1(b) depicts the XRD patterns of all the composite samples recorded in 2θ range of 10°–80°. The characteristics peaks were identified and well indexed with the corresponding miller planes of the samples as matched with the standard JCPDS (Joint Committee on Powder Diffraction Standards) data files. From the Fig. 1(a) it can be observed that raw MWCNTs show a characteristics peak at 26.28° ($d = 3.3883$), which corresponds to the (002) plane of the interplanar hexagonal carbon and also a peak at 42.65° which corresponds to (101) plane (JCPDS: 89-8487). The XRD pattern of graphene oxide depict the characteristics peak at $2\theta = 10.65°$ ($d = 8.2961$) which corresponds to (002) plane indicating the oxidation of graphene and the presence of a small peak at $2\theta = 26.46°$ concludes the presence of small amount of graphene in the oxide material (JCPDS: 87-0712).[23] The obtained XRD patterns of ferrite nanoparticles are completely consistent with their cubic inverse-spinel structure having diffraction peaks at $2\theta \sim 30.2°$, 35.5°, 43.1°, 57.0° and 62.5°, which correspond to the (220), (311), (400), (511) and (440) crystal planes of ferrite nanoparticles, (JCPDS: 75-0033).

The crystallite size of the nanocrystalline ferrites was calculated by Scherer's equation, $D = 0.9 \times \lambda/\beta \times \cos\theta$, where the wavelength of the X-ray is λ, β is the full width of the diffraction line at half of the maximum intensity, and θ is Bragg's angle.

Table 1 Structural parameters of ferrite nanoparticles computed from XRD patterns

Sample	Crystallite size using XRD (nm)	Lattice constant (Å)	X-ray density (g cm^{-3})	Particle size using TEM (nm)
$Ni_{0.7}Zn_{0.3}Fe_2O_4$	16	8.3687	5.35	19
$Co_{0.7}Zn_{0.3}Fe_2O_4$	18	8.3906	5.33	21

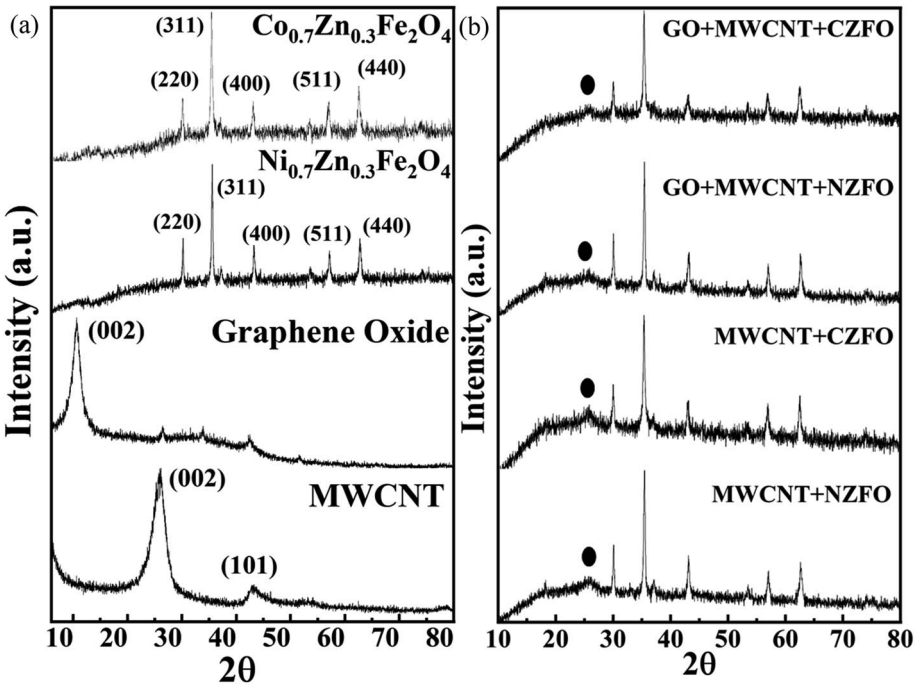

Fig. 1 Structural analysis curves with (a) XRD patterns of MWCNT, GO, NZFO and CZFO, (b) XRD patterns of composite samples (● peak corresponding MWCNT).

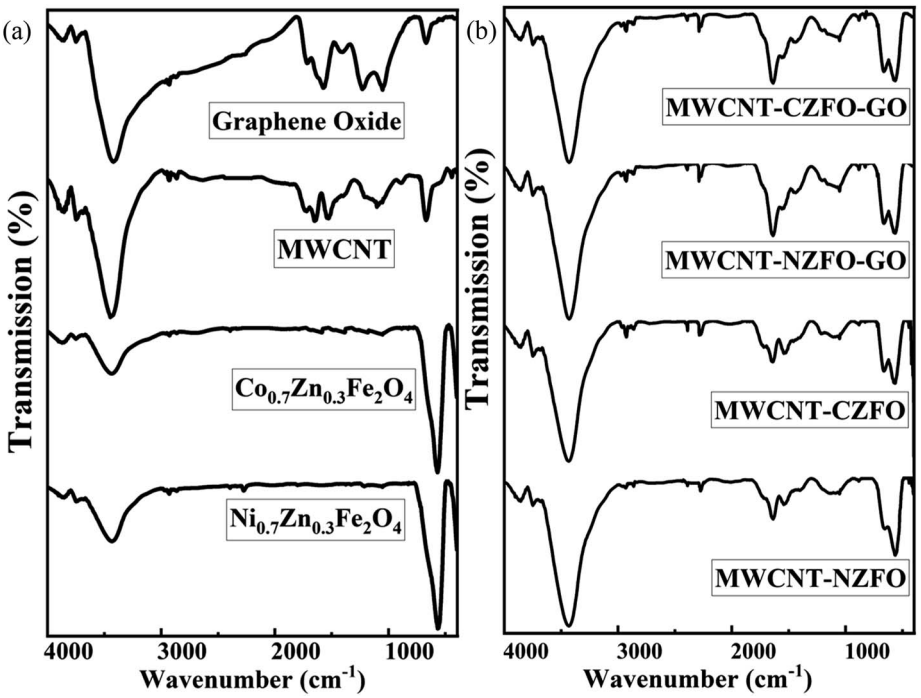

Fig. 2 FTIR spectra of (a) pristine and (b) composite samples in wave region of 400–4000 cm^{-1} recorded in transmission mode.

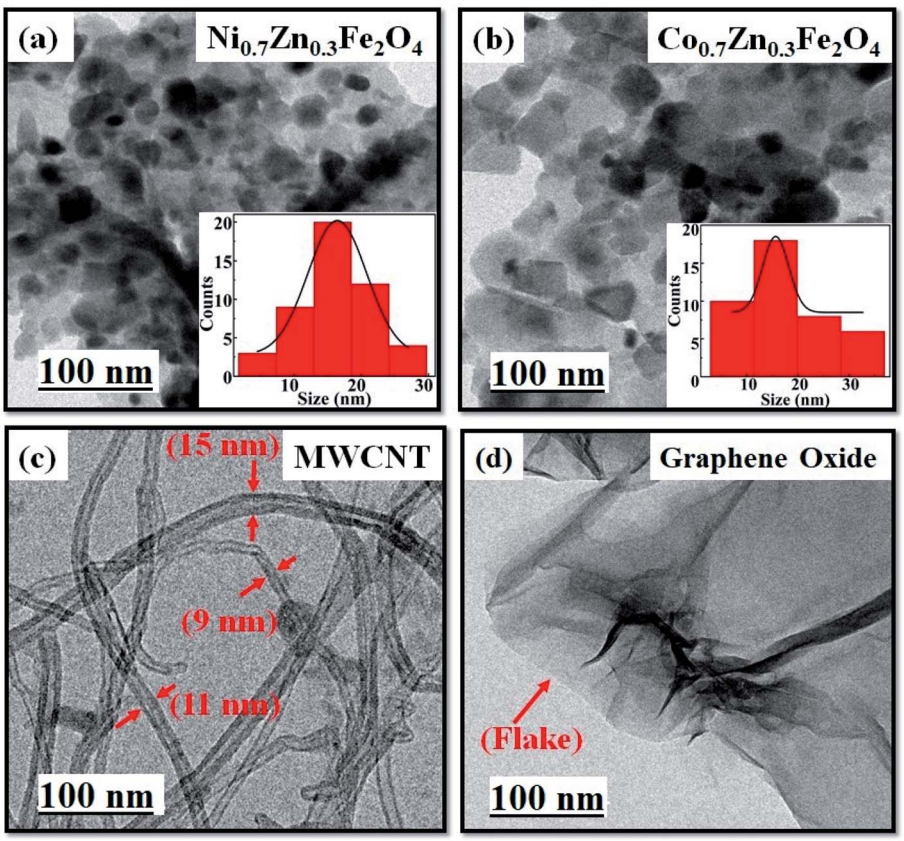

Fig. 3 HRTEM images of (a) NZFO, (b) CZFO (inset showing size distribution), (c) MWCNT and (d) GO showing their surface morphology and structural appearance.

The crystallite size of NZFO and CZFO samples is found to be 16 nm and 18 nm respectively. The X-ray density of the ferrite nanoparticles has also been computed by using the formula $\rho = 8M/Na^3$, and is observed to be 5.30 g cm^{-3} for NZFO and 5.32 g cm^{-3} for CZFO sample. The lattice constant for the cubic structure of nanocrystalline NZFO and CZFO samples is calculated as shown in Table 1.

XRD patterns of composite samples shown in Fig. 1(b), with the characteristics peaks of ferrites, MWCNT and graphene oxide which confirms the formation of hybrid phase structure in the composites with presence of both host matrix as well as filler particles. Meanwhile, no diffraction peak of graphite (~26°) can be observed in the hybrid nanocomposites, which indicates the accumulation of GO nanopowder remarkably intimidated by the incorporated ferrite nanoparticles.[24] Additionally, it can also be observed that the peaks also got slightly shifted to higher degrees indicating the enhancement in crystalline nature of composite samples with the addition of ferrite particles.

3.2 Infrared spectroscopy

FTIR spectroscopy is a powerful technique to characterize the characteristics vibrational bands/modes within the material and presence of various functional groups associated the bonds in the compound. Fig. 2(a) shows the FT-IR spectra for pristine NZFO, CZFO, MWCNT and graphene oxide while Fig. 2(b) displays NZFO–MWCNT, CZFO–MWCNT, MWCNT–NZFO–GO and MWCNT–CZFO–GO composite samples in a wavenumber range of 4000–400 cm^{-1}. From Fig. 2(a) it is clear that the ferrite nanoparticles have their characteristics peaks band at 400 cm^{-1} and 560 cm^{-1} corresponding to their octahedral and tetrahedral site vibrational modes. From Fig. 2(a), it can also be stated that IR spectra for MWCNT display a strong and broad peak around 3430 cm^{-1}, which corresponds to the stretching mode of the O–H group. The bands around 2950 and 2830 cm^{-1} are attributed to the asymmetric (aCH_2) and symmetric (sCH_2) stretching of C–H bond and the peak at 1630 cm^{-1} is due to the C–C stretching mode. In MWCNT, the peak at 1384 cm^{-1} is due to C–OH stretching vibrations and the peak at 1043 cm^{-1} is due to C–O stretching vibrations. The IR spectra of graphene oxide confirm the oxidised state of graphite or phase confirmation of graphene oxide with the characteristics bands at 3363 cm^{-1} corresponds to the O–H bond tension vibration, which is accompanied by the C–OH band at 1151 cm^{-1} due to the hydroxyl groups of the GO. At 1651 cm^{-1} the tension band C=C and at 1078 cm^{-1} the C–O–C band appears. It can be observed from Fig. 2(b) that all samples display an intense and wide peak around 3433 cm^{-1}, which corresponds to the stretching vibrational mode of the O–H group associated with C–OH groups and water molecules on the nanotubes surface while the peak at 3745 cm^{-1} is attributed to the free hydroxyl groups.[25] The characteristics peaks present around 2935 and 2864 cm^{-1} are ascribed to the asymmetric and symmetric vibrations of C–H bond and the peak appearing around 1638 cm^{-1} is due to the C=C stretching mode which corresponds to graphene.[26,27] In the spectra, obtained peaks around 1397 cm^{-1} and 1053 cm^{-1} are because of C–OH and C–O stretching vibrations in the multiwalled carbon nanotubes. The vibrational band present at around 1541 cm^{-1} can be attributed to the occurrence of carbonyl groups (C=O) in the composite materials for the host carbon based matrices. The incorporation of graphene oxide in the two composite samples is indicated by the appearance of

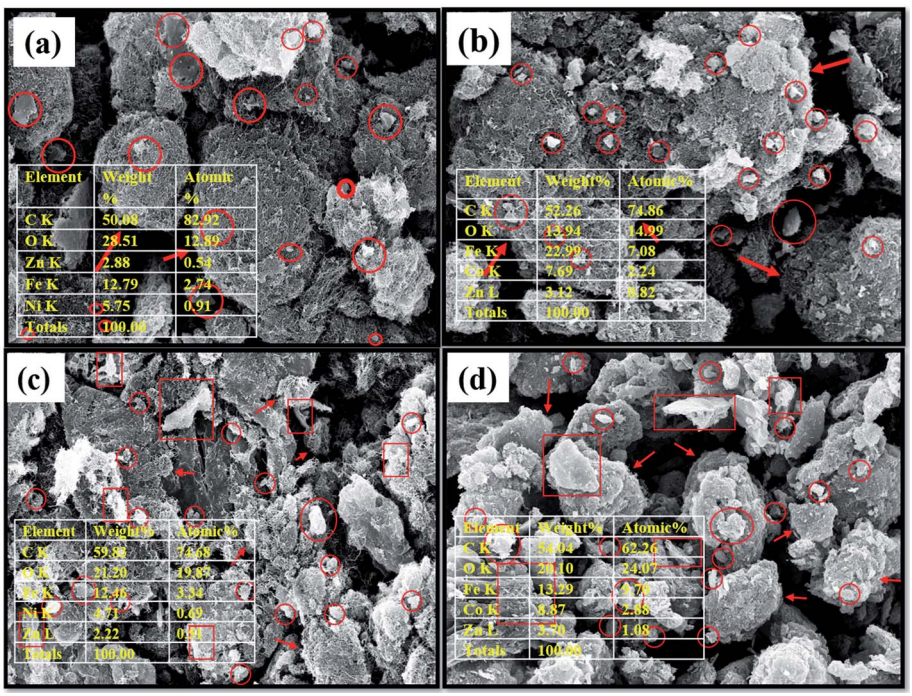

Fig. 4 SEM images with corresponding elemental composition table of composite samples with uniformly distributed ferrite nanoparticles (○), MWCNT (→) and GO (□).

new characteristics peaks at around 882 cm^{-1}, 1214 cm^{-1} and 1440 cm^{-1}, which can be associated to the C–N bond, C–O–C stretching vibrations and C–N vibrational modes respectively[28] The peaks observed at around 560 cm^{-1} and 655 cm^{-1} in all the samples corresponds to the octahedral and tetrahedral vibrational sites of ferrite nanoparticles having the inverse spinel structure which also confirms the incorporation of ferrite nanoparticles to all the composite samples. Hence the FTIR spectroscopy is in complete agreement with the compositional analysis of synthesized composite materials.

3.3 Surface morphology

Fig. 3(a) and (b) displays high resolution transmission electron microscope (HRTEM) images of $Ni_{0.7}Zn_{0.3}Fe_2O_4$ and $Co_{0.7}$-$Zn_{0.3}Fe_2O_4$ ferrite nanoparticles synthesized at 450 °C by using the sol–gel method. It was found that the average size of NZFO and CZFO nanoparticles was nearly equal to 19 nm and 21 nm respectively computed using ImageJ software. It can be observed from figure that the ferrite nanoparticles depicted a nanocluster morphology and they showed a relatively broad size distribution due to the agglomeration. TEM images for MWCNTs is depicted in Fig. 3(c). The images portray a clear morphology of these compounds. MWCNT exhibits the smooth surface with curled and entangled tubes. The observed diameter of carbon nanotubes from TEM image is in range of 8–15 nm while tubes are longer in length. The TEM image of the GO displayed in Fig. 3(c) clearly reveals the sheet-like structure as also reported by Satish B. *et al.*[29]

To study the microscopic morphology of composite samples, the SEM images and corresponding elemental composition table has been recorded and shown in Fig. 4. SEM micrographs of all composite samples clearly reflect that the ferrite nanoparticles were successfully decked in random arrangements on the outer surfaces of MWCNTs and later with a mixture of both MWCNT and graphene oxide. The MWCNTs have a tendency to form bundles and entanglements because of the van der Waals forces of attraction. The random dispersion of the MWCNT in the composite samples is clearly visible and the structure of MWCNTs is not damaged after all treatment.[30] As exhibited by SEM images, the surfaces of MWCNTs are encumbered with abundant ferrite nanoparticles and further twined with graphene oxide. It can be stated that the microstructural properties of MWCNT–ferrite–GO hybrid composites lead to formation of interconnected electromagnetically active network and structurally layered materials with conductive/magnetic/conductive structure which could enhance the internal reflection and absorption mechanism of EM waves.[31]

From the Fig. 5 it can be verified that the incorporation of composite material has formed a porous and uniform pattern in between the fibers of the fabrics which clearly indicates the presence of MWCNTs, ferrite nanoparticles and graphene oxide, leads to build an efficient shielding network. It is also clear that the deposition does not affect the fibers or the basic texture of the fabrics as the interlaced composite structure and fibers appearance are mostly distinguishable.

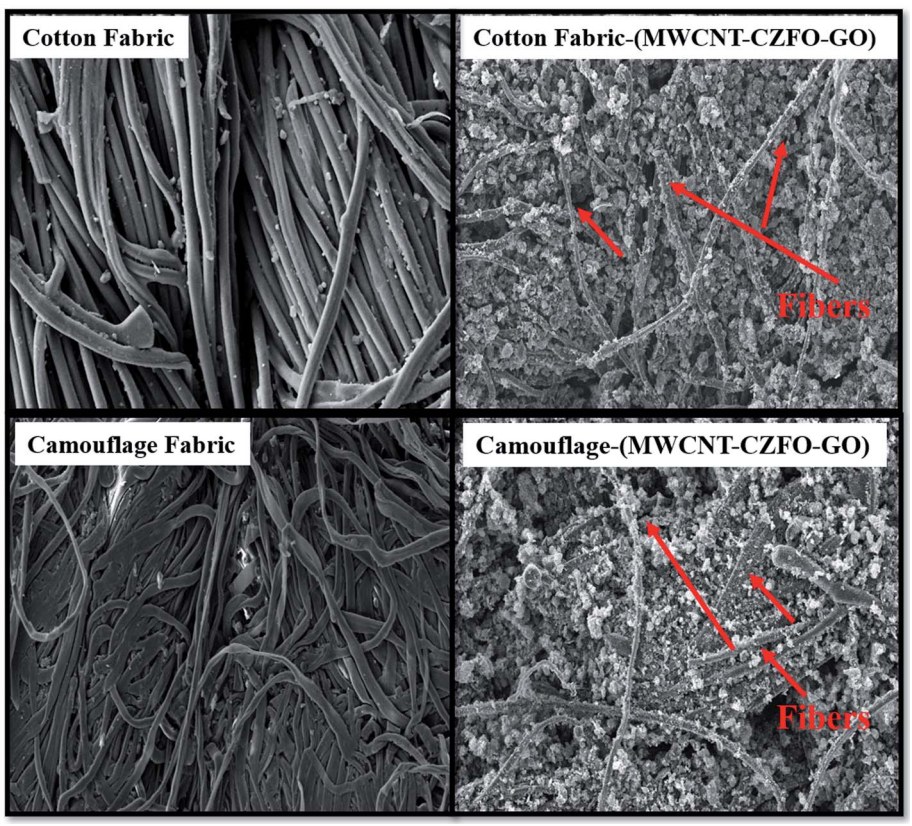

Fig. 5 SEM images of fabrics and MWCNT–CZFO–GO deposited fabric samples depicting the uniform dispersion on the surface.

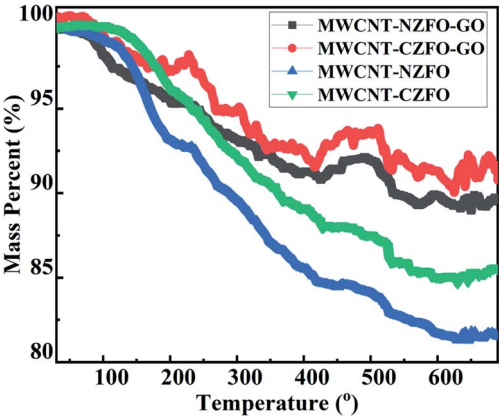

Fig. 6 Thermogravimetric analysis of composite samples from room temperature to 700 °C.

3.4 Thermal analysis

The TGA curves of the composite samples (MWCNT–NZFO, MWCNT–CZFO, MWCNT–NZFO–GO and MWCNT–CZFO–GO) are displayed in Fig. 6 where the mass variation has been carried out in temperature range of 30–700 °C at the rate 5 °C min^{-1}. The residues acquired form the composite samples MWCNT–NZFO, MWCNT–CZFO, MWCNT–NZFO–GO and MWCNT–CZFO–GO, are 82%, 87%, 89% and 91% respectively at 700 °C from the 100% at room temperature. It can be seen from curves that the weight loss of the composite samples is comprised of three stages in the measured temperature range. The first stage is observed when the temperature rises to 130 °C, a very small amount of weight loss takes place, which can be accredited to the evaporation of loss of the absorbed water molecules or volatile acidic residues present in the samples.[32] The second weight loss stage can be witnessed in the temperature range of about 250–430 °C due to the loss of bound water. The third step occurs in the temperature range of about 510–640 °C because of the decomposition of MWCNTs. It can be stated that this small weight loss or high thermal stability of the composite samples in this temperature range is due to the presence of thermally more stable MWCNTs which enhances the poor thermal behaviour of ferrite nanoparticles.[33] Further increase in thermal stability of MWCNT and GO incorporated composite samples is also due to an enhancement in degree of graphitization, which lessen the number of edge carbon atoms accountable for oxidation reaction.[34]

3.5 Magnetic properties

Fig. 7(a) shows the room temperature magnetic hysteresis loops of the zinc doped nickel and cobalt ferrite nanoparticles recorded in the field range of ±1 T. The saturation magnetization, coercivity and remanence of the samples are depicted in Table 2, which clearly portrays the ferromagnetic behaviour of the ferrite nanoparticles. Magnetic moment of ferrites depends on the magnetic ions in tetrahedral and octahedral sites inverse spinel nature of ferrites. The doping of zinc ions in cobalt and nickel ferrites change the arrangement of magnetic ions at each site (tetrahedral and octahedral) which in turn result to change in the net magnetic moment of the samples. The process can be accredited to the fact that the zinc ions replaced Ni/Co ions and engaged tetrahedral sites, displacing Fe^{3+} ions from tetrahedral

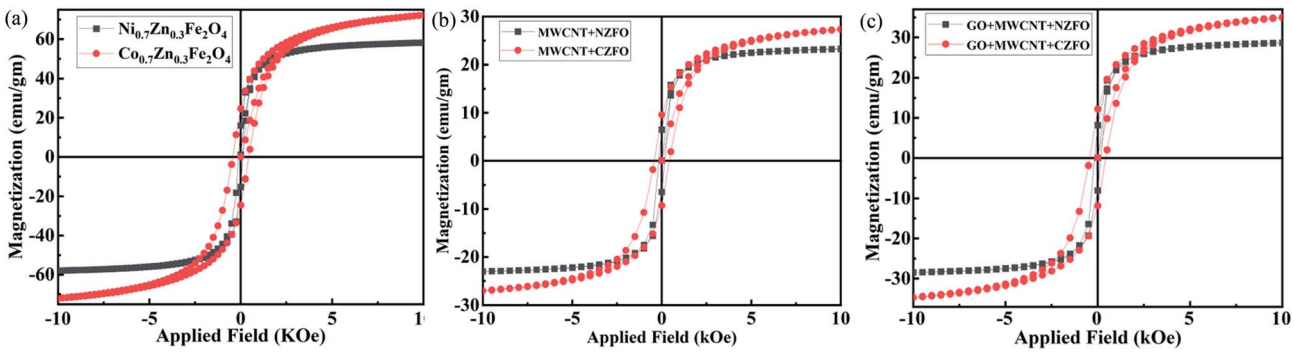

Fig. 7 Magnetic hysteresis loops of (a) zinc doped nickel and cobalt ferrite, (b) MWCNT–ferrite composites and (c) MWCNT–ferrite–GO composites recorded at room temperature.

Table 2 Magnetic parameters of pristine and composite samples evaluated from the hysteresis loops

Sample	Saturation magnetization (emu per g)	Remanent magnetization (emu per g)	Coercivity (Oe)
NZFO	58.2	15.9	115.6
CZFO	72.3	24.7	406.3
MWCNT–NZFO	26.5	7.6	165.7
MWCNT–CZFO	30.2	10.5	431.8
MWCNT–NZFO–GO	28.1	8.0	169.8
MWCNT–CZFO–GO	32.9	12.2	439.9

sites, increasing the concentration of Fe^{3+} ions in octahedral sites, which in turn enhances the magnetization of the Ni–Zn/Co–Zn ferrite.[35] This property helps Zn doped nickel and cobalt ferrite nanoparticles to achieve the high saturation magnetization of 58.2 emu per g and 72.3 emu per g which can be explained on the basis of Neel two sub lattice model.[45]

The magnetic response of ferrites based composites with graphene oxide and MWCNT, has been recorded in field range of ±1 T at room temperature. *M–H* loops of composite samples have been shown in Fig. 7(b) and (c) and corresponding magnetic parameters of the samples are listed in Tables 1–4. *M–H* curve of all the samples represented ferromagnetic hysteresis behaviour with their field dependent magnetization as a consequence of ferrite fillers in the composite samples. From Table 2, it can be seen that the coercivity (H_c) of composite samples has improved by small extent as compared to the pure ferrite nanoparticles while the saturation magnetization (M_s), remanent magnetization (M_r) values reduced due to the presence of nonmagnetic MWCNT and graphene oxide. When the NZFO ferrite particles were first incorporated to MWCNTs and further with MWCNT–GO having 50% weight ratio in the composite matrix, the saturation magnetization decreased from 58 to 26.5 emu per g and 58 to 28.1 emu per g for MWCNT–NZFO and MWCNT–NZFO–GO samples respectively. With the incorporation of CZFO ferrite particles to MWCNT and MWCNT–GO matrices, the magnetization reduced from 72.3 to 30.2 emu per g and 33.9 emu per g respectively. According to the equation, $M_s = \phi \times m_s$, where M_s denotes the magnetization of material, ϕ is related to the volume fraction of the magnetic particles in the material and m_s to the saturation moment of a single particle.[36] The M_s values are almost half of the pure ferrite samples which confirms the 1 : 1 weight ratio of ferrite particles to the host matrix as both MWCNT and graphene oxide are nonmagnetic in nature.[37,38] The coercivity value of the composites is observed to be increase from 406 to 439 Oe for CZFO composites and 115 Oe to 169 Oe for NZFO composites with the addition of MWCNT and GO which is due to the anisotropy energy. The carbon based matrices have the active functional groups and centres attached to them which in turn when mixed with the ferrite nanoparticles, increase the surface anisotropy energy due to which coercivity value increases.[39,40]

3.6 Electromagnetic shielding response

The shielding efficiency of any EM shielding material is the logarithmic proportion of incident and transmitted radiation power on its surface and is expressed in dB. A total SE of 30 dB, corresponding to 99.9% attenuation of electromagnetic waves, is viewed as an elegant level of SE for commercial applications.[41] As showed by Schelkunoff's theory, the interaction of any incident EM radiation with a material can be segmented into three parts, reflection, absorption and transmission of the radiation as they encounter with the material. Thus, a high shielding efficiency depends on less measure of transmitted radiation energy while largely dependent on reflection and absorption. The total SE attained by any shielding material is due to the contribution from reflection (SE_R), absorption (SE_A) and multiple reflections (SE_M),

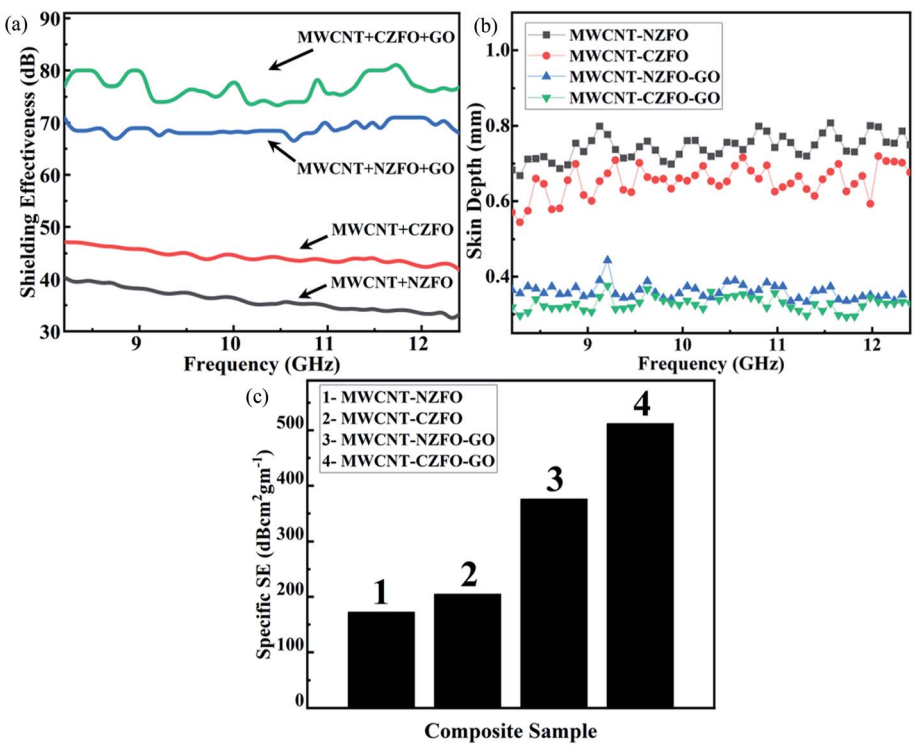

Fig. 8 Frequency dependence of (a) total shielding effectiveness, (b) skin depth and (c) variation of specific SE of composite samples in X-band frequency region.

$$SE = SE_R + SE_A + SE_M$$

The SE obtained as a result of reflection and absorption losses are given by the relationships,

$$SE_R = 10 \log(1 - R)$$

$$SE_A = 10 \log(1 - A_{eff}) = 10 \log(T/1 - R)$$

where R and T represent reflectance and transmittance, respectively. They can be described by the following equations:

$$T = [E_T/E_I]^2 = [S_{12}]^2 = [S_{21}]^2$$

$$R = [E_R/E_I]^2 = [S_{11}]^2 = [S_{22}]^2$$

A_{eff} represents the effective absorbance, which can be depicted as $A_{eff} = 1 - R - T/(1 - R)$ with respect to the power of the effectively incident electromagnetic radiation inside the shielding material. To determine the shielding performance of a material intrinsically, the specific shielding effectiveness per unit thickness can be computed for a material given as-

$$SSE = SE_T/(\text{density} \times \text{thickness})$$

Fig. 8(a) displays the total shielding effectiveness behaviour of composite samples in X-band frequency region with the sample thickness of 2.4 mm computed using the *S*-parameters recorded from vector network analyzer.

An effective EMI shielding material prerequisites the impedance matching condition, where the magnetic permeability value must be close to the electric permittivity value of the shielding material.[42] By introducing a suitable filler ratio of 1 : 1 for the ferrites and host matrix into the composite, the effect of impedance mismatch can be reduced and the absorption of EM radiations can be optimized. Also, the high amount of MWCNTs lead to dense conductive network with reduced hopping lengths which result in the enhancement of conduction losses inside the material. The observed highest shielding effectiveness values of all the samples are listed in Table 3. To compare the shielding performance of composite materials more comprehensively, the specific shielding effectiveness per unit thickness has been computed as shown in Table 3.

It can be depicted from the Table 3 that the MWCNT–CZFO–GO sample achieved the high SE (81.6 dB) and SSE/t (512.1 dB $cm^2\ g^{-1}$) values among all the composite samples. The addition of MWCNTs with the ferrite nanoparticles demonstrated a high shielding value of 47.1 dB (MWCNT–CZFO) and 40.8 dB (MWCNT–NZFO) which shows more than 99.999% of incident EM radiations are being attenuated by the composite materials. The multiwalled carbon nanotubes having high aspect ratio and high conductivity results to decrease in skin depth which in turn increase the attenuation capacity of the composite material and also provide a consistent conductive path for the dissipation of incident EM radiations resulting to high efficiency shielding performance. The addition of MWCNT has may enhanced the interface polarization, while dipole polarization increased due to interactions between MWCNT and ferrite nanoparticles.[43] MWCNTs are conductive in nature and have free electrons, thus the gathering of the charges at the interface of MWCNT with ferrite particles enhance the space charge polarizations which also contribute in EMI shielding phenomenon.[44] The incorporation of graphene oxide to the ferrite–MWCNT composites lead to their SE values to 81.6 dB and 71.1 dB for MWCNT–CZFO–GO and MWCNT–NZFO–GO samples respectively. The enhancement in the shielding efficiency can be ascribed to the development of a hybrid conducting network inside the composite materials, which serve as essential need for an efficient EMI shielding. There are two key reasons which can be stated for this, first is that the number of free electrons, functional groups and defects available to interact with the EM radiation are highly enhanced by addition of graphene oxide which cause the formation of electric dipoles which dissipate the incident EM energy due to their relaxation losses. Secondly, with the introduction of graphene oxide, electron hopping across the conductive network of MWCNTs and GO increases which causes the interfacial relaxation losses, converting more EM energy into heat energy. Also, maximum incident EM radiations are being trapped by the hybrid structure within the multiple heterogenous interfacial regions of nanosized ferrite particles acting as magnetization centres and conductive MWCNT and GO networks acting as polarization centres. The surface of MWCNTs is loaded with ferrite nanoparticles and further twinned with the graphene oxide, the ferrite nanoparticles serve as electron hoping/migration bridges between them leading to formation of small current networks which enhances the conduction losses inside the material.[45] In these kinds of the network structures, interaction of EM waves induced the micro currents, and as a result, electromagnetic energy gets vanished in the form of thermal energy. This process is followed by multiple absorptions and internal scattering of radiations in the interconnected network structure positioned by MWCNTs and the graphene oxide.[46] From our previous works, it is understood that the magnetization of ferrite nanoparticles in the composite materials tune up the absorption mechanism for the shielding phenomena and the absorption is directly dependent on the magnetic losses of the shielding material.[47] So, the addition of ferrite nanoparticles along with MWCNTs and MWCNT–GO give rise to shielding dominated by absorption rather than reflection and can be

Table 3 Total shielding effectiveness values for the composite samples

Sample	Total shielding effectiveness (dB)	SSE/thickness (dB $cm^2\ g^{-1}$)
MWCNT–NZFO	40.8	172.6
MWCNT–CZFO–CZFO	47.1	204.7
MWCNT–NZFO–GO	71.1	376.1
MWCNT–CZFO–GO	81.6	512.1

easily tuned with the help of magnetic behaviour of ferrite nanoparticles. It can be observed that the high magnetic response of CZFO nanoparticles than the NZFO nanoparticles has resulted in a better shielding effectiveness for CZFO based composites. The distinctive EMI shielding mechanism of the MWCNT–ferrite–GO composite samples can be recognized by the interconnected MWCNT–graphene oxide heterostructure.[48] The skin depth '*d*' of the composite samples which denotes the intensity of penetration of EM waves into the shield has been computed using the relation $d = 8.68 \times t/(SE_A)$, where t represents thickness of shield and SE_A the absorption shielding effectiveness. Critical thickness of the shield and its variation with frequency has been displayed in Fig. 8(b). It can be observed that MWCNT–CZFO–GO shows minimum skin depth. It reveals that the hybrid structure shield has the high absorption efficiency for the incident EM waves supported by the enhanced electric and magnetic losses. Table 4 exhibits the shielding effectiveness of some of carbon-based composite materials with current results, in various frequency regions reported in the literature, indicating the enhancement in shielding effectiveness due to the hybrid composite networks defined in this study. Thus, we can conclude that MWCNT–CZFO–GO composite samples exhibits highly efficient, light weight, minimal thickness and chemically stable EMI shielding material for attenuation of EM waves.

To explore the possibility of shield or reduce health hazards to human body associated with exposure to electromagnetic fields and in defence equipments, the composite material MWCNT–CZFO–GO was deposited on two different kind of fabrics (cotton fabric and camouflage fabric). The development of fabrics with such shielding effectiveness would be a handy tool for protection of humans and electronic appliances from EMI by acting as shield wall. Fig. 9(a) shows the variation of total shielding effectiveness of composite deposited fabrics with frequency in X-band frequency region (8–12 GHz). The differences in the fabrics are pattern density, blend ratios, and linear density of the warp and weft yams due to camouflage pattern as shown in Fig. 5. Due to the camouflage pattern incorporation of composite samples is dense and uniform which helped to achieve higher SE value 40.9 dB than cotton fabric of 28.6 dB. Thickness of both the fabrics was nearly 0.30 mm and there was no considerable variation in thickness of fabric samples after the uniform deposition of composite material. The synergy between MWCNT, GO and ferrites was positive in enhancing and providing a more reliable and consistent network for the radiation attenuation in the fabric samples.

Electromagnetic interference preventing is an increasing demand for the increasing adverse effects of EM pollution in daily human life. It is in that sense that the construction based materials which can effectively absorb the unwanted EM radiations would be of much attention due to increasing EMI pollution day by day. Cement and gypsum are thoroughly used, rich source and high environment adaptability materials used in engineering constructions. Cement has the slight conductive nature as compared with the gypsum. In the field of construction based shielding materials, the studies on incorporation of carbon and ferrite based materials are very few. Ferrites possess the high absorption properties as well as they can maintain the mechanical strength of these materials in order to achieve the high safety and stability.[56] Fig. 9(b) displays the electromagnetic shielding curves for the pure cement, pure gypsum and MWCNT–CZFO–GO incorporated cement and gypsum composites measured in X-band frequency region with a sample thickness of 2.5 mm. From Fig. 9(b) it is evident that the pure cement and gypsum show very low shielding behaviour with SE values of 5.9 dB and 10.1 dB respectively. With the incorporation of MWCNT–CZFO–GO composite sample in 1 : 1 weight ratio with cement and gypsum, the resulting materials portrayed a very high shielding attenuation response achieving the SE values of 52.3 dB for cement based composite and 31.4 dB for gypsum based composite material. The high value cement based composite material as compared to gypsum may be due to the conductive nature of cement which also contributes to the resulting shielding mechanism of the composite samples. Also, cement may have some absorbing properties due to presence of some metal oxide and minerals in it.[57] The existence of conducting MWCNT and GO and magnetic losses by ferrite nanoparticles in the cement or gypsum matrix plays a vital role in the enrichment of incident EM wave absorption. The achieved result of high shielding effectiveness of composite based

Table 4 Comparison of EMI shielding performance of different carbon-based composite materials reported in literature and current work

Composite material	Shielding effectiveness (dB)	Thickness (mm)	Frequency region (GHz)	Reference
MWCNT/$Ni_{0.7}Zn_{0.3}Fe_2O_4$	SE = 40.8	2.4	8.2–12.4	Present work
MWCNT/$Co_{0.7}Zn_{0.3}Fe_2O_4$	SE = 47.1	2.4	8.2–12.4	Present work
MWCNT/$Ni_{0.7}Zn_{0.3}Fe_2O_4$/GO	SE = 71.1	2.4	8.2–12.4	Present work
MWCNT/$Co_{0.7}Zn_{0.3}Fe_2O_4$/GO	SE = 81.6	2.4	8.2–12.4	Present work
$Co_{0.2}Ni_{0.4}Zn_{0.4}Fe_2O_4$/graphene	RL = 53.0	3.1	2–18	49
CNT/GNS@$CoFe_2O_4$ composite aerogels	SE = 29.1	3.0	2–18	50
MWCNT/MnZn ferrite/epoxy	SE = 44	2.0	8.2–12.4	51
rGO–CF/polyester	SE = 37.8	2.0	8.2–12.4	52
FeNi/$NiFe_2O_4$/NiO/CNF	RL = 37.4	2.0	12–18	53
$NiFe_2O_4$/rGO	SE = 39.7	3.0	8.2–12.4	54
Fe_3O_4/PPY/CNT	SE = 26	3.0	8.2–12.4	55
rGO/Fe_3O_4/PANI	SE = 51	2.5	8.2–12.4	2

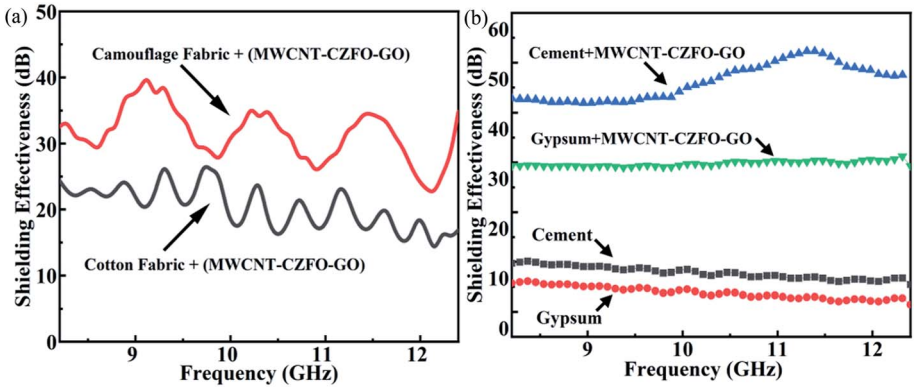

Fig. 9 EMI shielding applications of MWCNT–CZFO–GO composite incorporated to (a) cotton and camouflage fabric, (b) cement and gypsum material.

construction materials proposes that this hybrid structured composite material can serve as high potential candidate for future building construction material for electromagnetic shielding effectiveness applications.

4. Conclusions

Zinc doped nickel ferrite and cobalt ferrite nanoparticles (~20 nm) were synthesized by using the sol–gel method and further were chemically blended with carbon based MWCNT and MWCNT–GO host matrix for the composite samples. The spinel phase of the synthesized ferrite nanoparticles and the hybrid structure of composite samples was established by the XRD patterns with no impure peaks. SEM images also indicated effective dispersion of MWCNTs with ferrite nanoparticles in the composite samples while the fabrics deposited with the composite sample showed a well-structured morphology. The FTIR spectra of composite samples confirmed the structural presence of both ferrites as well as carbon-based materials showing all the vibrational bands and functional groups. Ferrite nanoparticles with high magnetization incorporated in non-magnetic MWCNT and MWCNT–GO which also exhibits good magnetic behaviours. The addition of GO with the MWCNT–ferrite composites had a great influence on EM wave attenuation performance of composite samples where maximum value of shielding effectiveness and specific shielding effectiveness is 81.6 dB and 512.1 dB cm^2 g^{-1} at thickness of 2.4 mm achieved for the composite MWCNT–CZFO–GO at frequency of 11.7 GHz in X-band frequency region. The other composite samples, MWCNT–NZFO, MWCNT–CZFO and MWCNT–CZFO–GO reached high SE values of 40.8 dB, 47.1 dB and 71.1 dB. This work provides an ingenious and effective approach to fabricate a high potential and excellent EM absorbing materials with light weight, strong absorption capability and wide absorption bandwidth. The development and application of construction based materials and clothes with high EMI shielding capabilities are urgently needed due to increasing worsened electromagnetic environment. MWCNT–CZFO–GO based cement composites, gypsum composites, cotton fabrics and camouflage fabrics yielded a high EMI shielding effectiveness of 52.3 dB, 31.4 dB, 40.9 dB and 28.6 dB respectively providing a new direction to control the adverse electromagnetic functions in human life.

Author contributions

Sumit Kumar: conceptualization, methodology, formal analysis, data curation, software, investigation, writing – original draft. Rajan Walia: validation, investigation, resources, writing – original draft. Ashwani Kumar: validation, formal analysis, resources. Vivek Verma: conceptualization, methodology, resources, writing – review & editing, supervision, project administration.

Conflicts of interest

There are no conflicts to declare.

Acknowledgements

Authors of this work are grateful to the Principal, Hindu College, University of Delhi and Head, Department of Physics and Astrophysics, University of Delhi. We acknowledge the University Science Instrumental Centre (USIC) and Prof. Vinay Gupta, University of Delhi for the characterization facilities and valuable suggestions regarding the present work. Author Sumit Kumar is thankful to the Council of Scientific and Industrial Research (CSIR) for providing the senior research fellowship (File No. 09/045(1578)/2018-EMR-I) for the necessary financial support and to carry out this research.

References

1 Z. Chen, C. Xu, C. Ma, W. Ren and H.-M. Cheng, Lightweight and flexible graphene foam composites for high-performance electromagnetic interference shielding, *Adv. Mater.*, 2013, **25**, 1296–1300.

2 A. P. Singh, M. Mishra, P. Sambyal, B. K. Gupta, B. P. Singh, A. Chandra, *et al.*, Encapsulation of c-Fe_2O_3 decorated reduced graphene oxide in polyaniline core–shell tubes as an exceptional tracker for electromagnetic environmental pollution, *J. Mater. Chem. A*, 2014, **2**, 3581–3593.

3 H. Vasquez, L. Espinoza, K. Lozano, H. Foltz and S. Yang, Simple Device for Electromagnetic Interference Shielding Effectiveness Measurement, *IEEE EMC Soc. Newsletter*, 2009, **220**, 62–68.

4 X. W. Yin, L. Kong, L. T. Zhang, L. F. Cheng, N. Travitzky and P. Greil, Electromagnetic properties of SieCeN based ceramics and composites, *Int. Mater. Rev.*, 2014, **59**, 326–355.

5 M. Zhang, C. Han, W.-Q. Cao, M.-S. Cao, H.-J. Yang and J. Yuan, A Nano–Micro Engineering Nanofiber for Electromagnetic Absorber, Green Shielding and Sensor, *Nano-Micro Lett.*, 2020, **13**, 27.

6 S. Biswas, G. P. Kar and S. Bose, Attenuating Microwave Radiation by Absorption through Controlled Nanoparticle Localization in PC/PVDF Blends, *Phys. Chem. Chem. Phys.*, 2015, **17**, 27698–27712.

7 M. Cao, X. Wang, W. Cao, X. Fang, B. Wen and J. Yuan, Thermally Driven Transport and Relaxation Switching Self-Powered Electromagnetic Energy Conversion, *Small*, 2018, **14**, 1800987.

8 S. Umrao, T. K. Gupta, S. Kumar, V. K. Singh, M. K. Sultania, J. H. Jung, I. K. Oh and A. Srivastava, Microwave-Assisted Synthesis of Boron and Nitrogen Co-Doped Reduced Graphene Oxide for the Protection of Electromagnetic Radiation in Ku-Band, *ACS Appl. Mater. Interfaces*, 2015, **7**, 19831–19842.

9 R. Kumaran, S. D. kumar, N. Balasubramanian, M. Alagar, V. Subramanian and K. Dinakaran, Enhanced Electromagnetic Interference Shielding in Au–MWCNT Composite Nanostructure Dispersed PVDF Thin Films, *J. Phys. Chem. C*, 2016, **120**, 13771–13778.

10 A. P. Singh, B. K. Gupta, M. Mishra, Govind, A. Chandra and R. B. Mathur, Multiwalled carbon nanotube/cement composites with exceptional electromagnetic interference shielding properties, *Carbon*, 2013, **56**, 86–96.

11 R. C. Che, L. M. Peng, X. F. Duan, Q. Chen and X. L. Liang, Microwave absorption enhancement and complex permittivity and permeability of Fe encapsulated within carbon nanotubes, *Adv. Mater.*, 2004, **16**, 401–405.

12 B. Wen, X. X. Wang, W. Q. Cao, H. L. Shi, M. M. Lu and G. Wang, Reduced graphene oxides: the thinnest and most lightweight materials with highly efficient microwave attenuation performances of the carbon world, *Nanoscale*, 2014, **6**, 5754–5761.

13 G. Wang, Z. Gao, S. Tang, C. Chen, F. Duan, S. Zhao, S. Lin, Y. Feng, L. Zhou and Y. Qin, Microwave Absorption Properties of Carbon Nanocoils Coated with Highly Controlled Magnetic Materials by Atomic Layer Deposition, *ACS Nano*, 2012, **6**, 11009–11017.

14 Y. Yang, M. Li, Y. Wu, T. Wang, E. S. G. Choo, J. Ding, B. Zong, Z. Yang and J. Xue, Nanoscaled Self-Alignment of Fe_3O_4 Nanodiscs in Ultrathin rGO Films with Engineered Conductivity for Electromagnetic Interference Shielding, *Nanoscale*, 2016, **8**, 15989–15998.

15 J. Shen, Y. Hu, M. Shi, N. Li, H. Ma and M. Ye, One step synthesis of graphene oxide–magnetic nanoparticle composite, *J. Phys. Chem. C*, 2010, **114**, 1498–1503.

16 S. Kumar, P. Kumar, A. Ohlan and V. Verma, Improved Electromagnetic Interference Shielding Response of Polyaniline Containing Magnetic Nano-Ferrites, *J. Supercond. Novel Magn.*, 2019, **33**, 1187–1198.

17 Y. Li, M. Yu, P. Yang and J. Fu, Enhanced Microwave Absorption Property of Fe Nanoparticles Encapsulated within Reduced Graphene Oxide with Different Thicknesses, *Ind. Eng. Chem. Res.*, 2017, **56**, 8872–8879.

18 M.-S. Cao, W.-L. Song, Z.-L. Hou, B. Wen and J. Yuan, The effects of temperature and frequency on the dielectric properties, electromagnetic interference shielding and microwave-absorption of short carbon fiber/silica composites, *Carbon*, 2010, **48**, 788–796.

19 Z. Jia, Z. Gao, K. Kou, A. Feng, C. Zhang, B. Xu and G. Wu, Facile synthesis of hierarchical a-site cation deficiency perovskite La_xFeO_{3-y}/RGO for high efficiency microwave absorption, *Compos. Commun.*, 2020, **20**, 100344.

20 S. Kumar, P. Kumar, R. Gupta and V. Verma, Electromagnetic interference shielding behaviors of in situ polymerized ferrite-polyaniline nano-composites and ferrite–polyaniline deposited fabrics in X-band frequency range, *J. Alloys Compd.*, 2021, 158331.

21 Q. Liu, X. Xu, W. Xia, R. Che, C. Chen, Q. Cao and J. He, Dependency of magnetic microwave absorption on surface architecture of $Co_{20}Ni_{80}$ hierarchical structures studied by electron holography, *Nanoscale*, 2015, **7**, 1736–1743.

22 Q. Liu, Q. Cao, X. Zhao, H. Bi, C. Wang, D. Wu and R. Che, Insights into size-dominant magnetic microwave absorption properties of CoNi micro-flowers via off-axis electron holography, *ACS Appl. Mater. Interfaces*, 2015, **7**, 4233–4240.

23 H. He and C. Gao, Supraparamagnetic, conductive and processable multifunctional graphene nanosheets coated with high density Fe_3O_4 nanoparticles, *ACS Appl. Mater. Interfaces*, 2010, **2**, 3201–3210.

24 J. He, X. Wang, Y. Zhang and M. Cao, Small magnetic nanoparticles decorating reduced graphene oxides to tune the electromagnetic attenuation capacity, *J. Mater. Chem. C*, 2016, **4**, 7130–7140.

25 S. Verma, H. P. Mungse, N. Kumar, S. Choudhary, S. L. Jain, B. Sain and O. P. Khatri, Graphene oxide: an efficient and reusable carbocatalyst for aza-Michael addition of amines to activated alkenes, *Chem. Commun.*, 2011, **47**, 12673–12675.

26 S. Wang, D. Yu, L. Dai, D. W. Chang and J.-B. Baek, Polyelectrolyte-Functionalized Graphene as Metal-Free Electrocatalysts for Oxygen Reduction, *ACS Nano*, 2011, **5**, 6202.

27 L. Kunping, Z. Jingjing, Y. Guohai, W. Chunming and Z. Jun-Jie, Direct electrochemistry and electrocatalysis of hemoglobin based on poly(diallyldimethylammonium chloride) functionalized graphene sheets/room temperature ionic liquid composite film, *Electrochem. Commun.*, 2010, **12**, 402.

28 L.-L. Li, K.-P. Liu, G.-H. Yang, C.-M. Wang, J.-R. Zhang and J.-J. Zhu, Fabrication of Graphene–Quantum Dots Composites for Sensitive Electrogenerated

Chemiluminescence Immunosensing, *Adv. Funct. Mater.*, 2011, **21**, 869.

29 B. Satish, K. V. Rao, C. H. Shilpa Chakra and T. Tejaswi, Synthesis and characterization of graphene oxide and its antimicrobial activity against *Klebsiella* and *Staphylococcus*, *Int. J. Adv. Biotechnol. Res.*, 2013, **4**, 142–146.

30 Y. Li, Preparation, magnetic and electromagnetic properties of polyaniline/strontium ferrite/multiwalled carbon nanotubes composite, *Appl. Surf. Sci.*, 2012, **258**, 3659–3666.

31 Z. Durmus, D. Ali and H. Kavas, Synthesis and characterization of structural and magnetic properties of graphene/hard ferrite nanocomposites as microwave-absorbing material, *J. Mater. Sci.*, 2015, **50**, 1201–1213.

32 A. G. MacDiarmid and A. J. Epstein, Secondary doping in polyaniline, *Synth. Met.*, 1995, **69**, 85–92.

33 H. Qiu, S. H. Qi, D. H. Wang, J. Wang and X. M. Wu, Synthesis of polyaniline nanostructures via soft template of sucrose octaacetate, *Synth. Met.*, 2010, **160**, 1179–1183.

34 C. L. Yuan, Y. S. Hong and C. H. Lin, Synthesis and characterization of $Sr(ZnZr)_xFe_{12-2x}O_{19}$–PANI composites, *J. Magn. Magn. Mater.*, 2011, **323**, 1851–1854.

35 D. R. Patil and B. K. Chougule, Effect of copper substitution on electric and magnetic properties of $NiFe_2O_4$ ferrite, *Mater. Chem. Phys.*, 2009, **117**, 35–40.

36 S. Thomas, N. Kalarikkal, M. Jaroszewski and J. P. Jose, *Advanced polymeric materials: from macro- to nano-length scales*, Apple Academic Press, 2015, p. 116.

37 J. Jiang, L. H. Ai and L. C. Li, Multifunctional polypyrrole/strontium hexaferrite composite microspheres: preparation, characterization, and properties, *J. Phys. Chem. B*, 2009, **113**, 1376–1380.

38 P. Yu, L. Matzui, L. Vovchenko, P. Yu, P. Scharff and U. Ritter, The effect of boron nitride on electrical conductivity of nanocarbon–polymer composites, *J. Mater. Sci.*, 2014, **49**, 2098–2105.

39 M. Y. Li and G. D. Li, *Ferrite Physics* Science Press, Beijing, 1978.

40 J. R. Martínez, J. Román de Alba, I. G. Blanco-Esqueda, A. Guerrero-Serrano and G. Ortega-Zarzosa, Coercivity values enhancement by incorporation of magnetic powders in inorganic matrix hosts, *New J. Glass Ceram.*, 2013, **3**, 1–5.

41 P. Liu, Z. Yao, V. M. H. Ng, J. Zhou, L. B. Kong and K. Yue, Facile synthesis of ultrasmall Fe_3O_4 nanoparticles on MXenes for high microwave absorption performance, *Composites, Part A*, 2018, **115**, 371–382.

42 A. M. Gama, M. C. Rezende and C. C. Dantas, Dependence of microwave absorption properties on ferrite volume fraction in MnZn ferrite/rubber radar absorbing materials, *J. Magn. Magn. Mater.*, 2011, **323**, 2782–2785.

43 B. Wen, M. Cao, M. Lu, W. Cao, H. Shi and J. Liu, Reduced graphene oxides: light-weight and high-efficiency electromagnetic interference shielding at elevated temperatures, *Adv. Mater.*, 2014, **26**, 3484–3489.

44 B. Quan, X. Liang, G. Ji, J. Ma, P. Ouyang, H. Gong, G. Xu and Y. Du, Strong electromagnetic wave response derived from the construction of dielectric/magnetic media heterostructure and multiple interfaces, *ACS Appl. Mater. Interfaces*, 2017, **9**, 9964–9974.

45 B. Zhao, L. Liang, J. Deng, Z. Bai, J. Liu, X. Guo, K. Gao, W. Guo and R. Zhang, 1D Cu@Ni nanorods anchored on 2D reduced graphene oxide with interfacial engineering to enhance microwave absorption properties, *CrystEngComm*, 2017, **19**, 6579–6587.

46 P. Liu, V. M. H. Ng, Z. Yao, J. Zhou, Y. Lei and Z. Yang, Facile synthesis and hierarchical assembly of flowerlike NiO structures with enhanced dielectric and microwave absorption properties, *ACS Appl. Mater. Interfaces*, 2017, **9**, 16404–16416.

47 S. Kumar, P. Kumar, W. Rajan and V. Verma, Magnetization and thickness dependent microwave attenuation behavior of ferrite–PANI composites and embedded composite-fabrics prepared by in situ polymerization, *AIP Adv.*, 2021, **11**, 015106.

48 T. W. Lee, S. E. Lee and Y. G. Jeong, Highly effective electromagnetic interference shielding materials based on silver nanowire/cellulose papers, *ACS Appl. Mater. Interfaces*, 2016, **8**, 13123–13132.

49 H. Chen, S. Bai, S. Li, F. Huang, Y. Lu, L. Wang and H. Zhang, Facile synthesis RGO/MnO_x composite aerogel as high-efficient electromagnetic wave absorbents, *J. Alloys Compd.*, 2019, **773**, 980–987.

50 P. Liu, Y. Huang, J. Yan and Y. Zhao, Magnetic graphene@PANI@porous TiO_2 ternary composites for high-performance electromagnetic wave absorption, *J. Mater. Chem. C*, 2016, **4**, 6362–6370.

51 C. Phan, M. Mariatti and Y. Koh, *J. Magn. Magn. Mater.*, 2016, **401**, 472–478.

52 J. Chen, J. Wu, H. Ge, D. Zhao, C. Liu and X. Hong, *Composites, Part A*, 2016, **82**, 141–150.

53 Y. Shen, Y. Wei, J. Ma, Y. Zhang, B. Ji, J. Tang, L. Zhang, P. Yan and X. Du, Self cleaning functionalized FeNi/$NiFe_2O_4$/NiO/C nanofibers with enhanced microwave absorption performance, *Ceram. Int.*, 2020, **46**, 13397–13406.

54 M. Zong, Y. Huang, X. Ding, N. Zhang, C. Qu and Y. Wang, One-step hydrothermal synthesis and microwave electromagnetic properties of RGO/$NiFe_2O_4$ composite, *Ceram. Int.*, 2014, **40**, 6821–6828.

55 R. B. Yang, P. Reddy, C. J. Chang, P. A. Chen, J. K. Chen and C. C. Chang, Synthesis and characterization of Fe_3O_4/polypyrrole/carbon nanotube composites with tunable microwave absorption properties: role of carbon nanotube and polypyrrole content, *Chem. Eng. J.*, 2016, **285**, 497–507.

56 Y. Wu, Design and electromagnetic wave absorption properties of reduced graphene oxide/multi-walled carbon nanotubes/nickel ferrite ternary nanocomposites, *J. Alloys Compd.*, 2019, **784**, 887–896.

57 H. Guan, S. Liu, Y. Duan and Y. Zhao, Investigation of the electromagnetic characteristics of cement based composites filled with EPS, *Cem. Concr. Compos.*, 2007, **29**, 49–54.